The Generation, Turbulent Transfer and Deposition of the Sea-Salt Aerosol

STEPHEN D. BURK

Naval Environmental Prediction Research Facility, Monterey, CA 93943

(Manuscript received 23 April 1984, in final form 27 July 1984)

ABSTRACT

An atmospheric boundary layer (ABL) model is used to address problems involving the generation, turbulent transport, and deposition of giant sized (1–25 μm) sea-salt aerosol. The surface aerosol generation rate is taken from the production flux expressions developed by Monahan. A simplified second-moment closure formulation for turbulent transport is used, while dry deposition fluxes are computed as functions of Stokes' settling speed and the rate of inertial impaction of particles across the viscous sublayer.

Initially we investigate, starting from first principles, whether the model can develop reasonable sea-salt volume distributions at several different Beaufort wind forces. Using the empirical expressions for generation and deposition fluxes, we permit an initially aerosol-free ABL to fill by diffusion until the volume distributions approach equilibrium; we then compare these distributions with the classic Woodcock observations. Further experiments are conducted in which we explore the dynamic behavior of the aerosol spectra when winds are varying, and also we study vertical sea-salt profiles in a humid, trade wind ABL.

1. Introduction

The first detailed observations of the sea-salt aerosol size distribution were conducted by Woodcock (1950, 1953) and Woodcock and Gifford (1949). Since that time, marine aerosol research has blossomed into a large, wide-ranging field that has attracted a diversified, interdisciplinary group of researchers. The rapid growth of this field is not surprising considering that of all particulate matter cycled through the atmosphere, the largest component is sea salt (Blanchard, 1983). During its atmospheric cycle, the sea-salt aerosol plays a pivotal role in the mechanism of precipitation, in the reduction of marine optical and infrared transmissivity, in the ocean-to-air transport of bacteria, and can have a detrimental effect on ship turbines and other machinery, to name just some of its impacts on our environment. Knowledge of the sea-salt size distribution, and the manner and rate at which atmospheric processes can alter the character of this distribution are important in many of these fields.

One of the most striking features of aerosol spectra is the general similarity of their distributions for particles greater than about 0.5 micrometers in radius. The familiar Junge power law, $dN/d\log r \propto r^{-3}$, often is a good rough approximation despite order of magnitude differences in actual concentration. Friedlander (1960, 1977) developed a theory for broadly explaining these features by assuming that this region of the spectrum attains a state of dynamic equilibrium in which the rate at which coagulating particulates enter the small size end is equal to the net loss of sedimenting particles from the large size end. This local equilibrium can be attained only at points well removed from the sources of aerosol. This approach is of questionable value in describing marine sea-salt distributions where the surface acts as a continuous area source.

Junge (1957) made the first numerical investigation of the diffusional-filling of a clear boundary layer due to turbulent transport of an aerosol having a specified, uniform surface production flux. In his calculation, an eddy coefficient was specified, the aerosol were taken to have zero fall velocity, no aerosol growth was considered, and only the one-dimensional diffusion equation was numerically integrated. More recently Sato (1979), also using only the diffusion equation and a specified eddy coefficient, added the influences of sedimentation and a parameterized washout expression to study the dynamics of aerosol distributions.

In this paper we use a turbulence model of the marine boundary layer to examine the development of the sea-salt aerosol distribution. For the upward production flux at the sea surface, which is a function of radius and the surface wind stress, we use the empirical expression derived by Monahan *et al.* (1983a). Turbulent transfer is handled by a simplified second-moment closure turbulence model. The deposition flux is computed from an expression which is a function of the Stokes settling speed and rate of inertial impaction across the viscous sublayer, while sedimentation is computed using Kasten's (1969) expression for equilibrium aerosol size at the local relative humidity. For simplicity, we neglect continental aerosols in this study, and do not attempt to parameterize washout or rainout processes.

Our first task is to see whether this model, using empirical production, deposition, and turbulent transport expressions, can develop reasonable sea-salt aerosol distributions. Model experiments with steady winds of Beaufort 3, 5, and 7 are run until quasi-equilibrium volume distributions are developed and then the results are compared with the classic Woodcock distributions.

In a further set of experiments, we begin with the equilibrium distributions described above, and then require the wind speed to undergo either a ramp function increase or decrease during a three hour period. Once the wind is altered, numerous feedback mechanisms modify the character of the aerosol distribution. The turbulence intensity is altered, the surface aerosol generation flux changes, and even the deposition velocity is affected. The impact of all of these temporally varying processes upon the volume distribution is then analyzed.

The final numerical experiment examines the vertical distribution of sea-salt particles in a trade wind ABL in which the relative humidity has a maximum aloft just beneath the trade wind inversion.

2. Model description

a. The equation set

To describe the atmospheric dynamics and turbulence transport we use a model based on the second-moment closure formulations of Mellor and Yamada (1974). We have used this model for a large variety of purposes (Burk, 1977, 1980, 1981; Burk and Thompson, 1982) and found it to give generally reliable, physically realistic simulations of boundary layer behavior. In a recent model intercomparison study in which five different models made fog forecasts from a blind data set (i.e., initial and boundary conditions were supplied, but verifying conditions were not), this model was ranked first when forecasts were compared with the verifying soundings (Mack *et al.*, 1983). A review article by Mellor and Yamada (1982) covers a very wide and impressive list of phenomena that have been studied by researchers using models based on the Mellor and Yamada formulations. Remarkably, these geophysical modeling successes have been achieved using empirical closure constants derived solely from *neutral laboratory flow* data.

Making the boundary layer approximation in which divergences of horizontal fluxes are neglected in comparison to those in the vertical, and further neglecting horizontal advection results in a one-dimensional model in which the mean equations are

$$\frac{\partial U}{\partial t} = -\frac{\partial}{\partial z}\overline{wu} + f(V - V_g) - W\frac{\partial U}{\partial z}, \quad (1)$$

$$\frac{\partial V}{\partial t} = -\frac{\partial}{\partial z}\overline{wv} - f(U - U_g) - W\frac{\partial V}{\partial z}, \quad (2)$$

$$\frac{\partial \Theta_l}{\partial t} = -\frac{\partial}{\partial z}\overline{w\theta_l} - W\frac{\partial \Theta_l}{\partial z} + \dot{Q}_r, \quad (3)$$

$$\frac{\partial Q_w}{\partial t} = -\frac{\partial}{\partial z}\overline{wq_w} - W\frac{\partial Q_w}{\partial z}, \quad (4)$$

$$\frac{\partial N(r_i)}{\partial t} = -\frac{\partial}{\partial z}\overline{wn} - (W - W_f)\frac{\partial N(r_i)}{\partial z},^{1} \quad (5)$$

where upper case is used for mean quantities and lower case for turbulent fluctuations. The overbar refers to an ensemble average. Here $N(r_i)$ is the aerosol concentration at radius r_i, W_f the particulate fall speed (taken positive downward), and $\dot{Q}_r$ the radiative cooling/heating rate. The remaining symbols in these equations are conventional and are defined in the Appendix.

In second-order modeling, equations are developed to describe the dynamic behavior of the turbulent fluxes appearing in Eqs. (1)–(5). While these equations contain major production terms that require no modeling, they also contain further unknown terms involving triple-moment correlations, pressure-strain rate and pressure-scalar covariances, and molecular dissipation which do require parameterization. Mellor (1973) proposed a set of closure expressions for these terms, and in Mellor and Yamada (1974) the second-moment equations are systematically simplified based on the level of anisotropy of the flow. We use the level of sophistication termed "Level 3," which is one step removed from the full set of second-moment equations. Thus, we carry dynamic equations for turbulent kinetic energy, temperature variance, moisture variance, and temperature-moisture covariance:

$$\frac{\partial q^2}{\partial t} = \frac{\partial}{\partial z}\left(\gamma lq\frac{\partial q^2}{\partial z}\right) - 2\overline{uw}\frac{\partial U}{\partial z} - 2\overline{vw}\frac{\partial V}{\partial z} + 2\beta g\overline{w\theta_v} - \frac{2q^3}{B_1 l}, \quad (6)$$

$$\frac{\partial \overline{\theta_l^2}}{\partial t} = \frac{\partial}{\partial z}\left(\gamma lq\frac{\partial \overline{\theta_l^2}}{\partial z}\right) - 2\overline{w\theta_v}\frac{\partial \Theta_v}{\partial z} - \frac{2q\overline{\theta_v^2}}{B_2 l}, \quad (7)$$

$$\frac{\partial \overline{q_w^2}}{\partial t} = \frac{\partial}{\partial z}\left(\gamma lq\frac{\partial \overline{q_w^2}}{\partial z}\right) - 2\overline{wq_w}\frac{\partial Q_w}{\partial z} - \frac{2q\overline{q_w^2}}{B_2 l}, \quad (8)$$

$$\frac{\partial \overline{\theta_l q_w}}{\partial t} = \frac{\partial}{\partial z}\left(\gamma lq\frac{\partial \overline{\theta_l q_w}}{\partial z}\right) - \overline{w\theta_l}\frac{\partial Q_w}{\partial z} - \overline{wq_w}\frac{\partial \Theta_l}{\partial z} - \frac{2q}{B_2 l}\overline{\theta_l q_w}. \quad (9)$$

At Level 3, the time derivative and advective terms in the dynamic equations for Reynolds stress, and

[1] We actually solve Eq. (5) for a number of different radii bins which go into making up our aerosol distribution. We selected radii values r_i of 1, 2, 3, 4, 5, 7, 10, 15, 20, and 25 μm at a standard relative humidity of 80%.

heat and moisture flux are neglected based on a scale analysis. The resulting algebraic equations for the flux terms appearing in Eqs. (1–4) are

$$-\overline{uw} = \frac{3A_1 l}{q}\left[(\overline{w^2} - C_1 q^2)\frac{\partial U}{\partial z} - \beta g\overline{u\theta_v}\right], \quad (10)$$

$$-\overline{vw} = \frac{3A_1 l}{q}\left[(\overline{w^2} - C_1 q^2)\frac{\partial V}{\partial z} - \beta g\overline{v\theta_v}\right], \quad (11)$$

$$-\overline{w\theta_l} = \frac{3A_2 l}{q}\left(\overline{w^2}\frac{\partial \Theta_l}{\partial z} - \beta g\overline{\theta_v\theta_l}\right), \quad (12)$$

$$-\overline{wq_w} = \frac{3A_2 l}{q}\left(\overline{w^2}\frac{\partial Q_w}{\partial z} - \beta g\overline{\theta_v q_w}\right). \quad (13)$$

The vertical velocity variance appearing in Eqs. (10)–(13) is given by

$$\overline{w^2} = q^2/3 + \frac{2A_1 l}{q}\left(\overline{uw}\frac{\partial U}{\partial z} + \overline{vw}\frac{\partial V}{\partial z} + 2\beta g\overline{w\theta_v}\right). \quad (14)$$

In order to achieve a closed set of equations, the terms involving virtual potential temperature fluctuations θ_v have to be rewritten in terms of our independent variables, fluctuating liquid water potential temperature (θ_l) and fluctuating total moisture (q_w). This rather lengthy task is described by Yamada (1978).

Thus far we have not described our treatment of the aerosol flux term, $\overline{wn}$, appearing in Eq. (5). By taking moments of the instantaneous variables and performing an ensemble average, one could generate an exact dynamic equation for the flux components, $\overline{u_i n}$ (e.g., Donaldson, 1973). Newly appearing unknowns involving $\theta_v n$, $\overline{u_i u_j n}$, $n(\partial p/\partial x_i)$, and $(\partial u_i/\partial x_k)(\partial n/\partial x_k)$ then appear in this tensor equation and further expressions would need to be developed to attain a closed set of equations. However, we feel that these additional terms are currently too little understood to warrant this traditional second-order closure approach. Instead, we use the level 3 expression for heat flux to derive an effective eddy coefficient, K, for transport of a scalar. This effective eddy coefficient is then used to compute aerosol flux as $-\overline{wn} = K\partial N/\partial z$.

b. Boundary and initial conditions

Prognostic equations (1)–(9) are finite differenced in an implicit manner. Lower and upper boundary values of the momentum, heat, moisture, and aerosol fluxes appearing in Eqs. (1)–(5) must be incorporated into these difference equations. The surface fluxes of momentum, heat, and moisture are computed from surface layer similarity profiles (Businger, 1973). For the surface upward aerosol production flux we use an empirical expression developed by Monahan *et al.* (1983a), while for the sea-salt deposition we utilize an expression proposed by Lewellen and Sheng (1980). These aerosol fluxes are discussed further in the next section.

The lower boundary conditions for Eqs. (6)–(9) are found by assuming a production-dissipation balance near the surface and use of scaling parameters found from the similarity profiles (see Burk, 1980, for further description of how we compute u_* and θ_{v*}). For example, in the turbulent kinetic energy (TKE) equation (Eq. 6), shear and buoyant production of TKE are required to equal the viscous dissipation rate, that is

$$-\overline{uw}\frac{\partial U}{\partial Z} - \overline{vw}\frac{\partial V}{\partial Z} + \beta g\overline{w\theta_v} = q^3/(B_1 l). \quad (15)$$

In the surface layer, the fluxes can be expressed in terms of the scaling velocity u_* and scaling virtual temperature θ_{v*}, and the similarity expression for nondimensional wind shear, ϕ_m, may be used. Thus, we have

$$u_*^2\cos\alpha\left[\frac{u_*\cos\alpha}{kz}\phi_m(z/L)\right] + u_*^2\sin\alpha\left[\frac{u_*\sin\alpha}{kz}\phi_m(z/L)\right] - \beta g\theta u_*\theta_{v*} = \frac{q^3}{(B_1 l)}, \quad (16)$$

where L is the Monin-Obukhov length and α the angle of the surface stress relative to the x-axis. Our boundary condition on TKE therefore is

$$q^2 = \left[B_1 l\left(\frac{u_*^3\phi_m}{kz} - \beta g u_*\theta_{v*}\right)\right]^{2/3}. \quad (17)$$

The surface roughness length z_0 is computed from Charnock's relationship $z_0 = 0.05u_*^2/g$, unless this value is less than the viscous sublayer thickness, $\delta = \nu/(ku_*)$. In that event we use δ as the roughness length.

The upper boundary of the model is selected in such a way that it lies well within the free atmosphere; therefore, turbulent fluxes at the top of the grid are set to zero. The mean wind shear is set to zero at the upper boundary, while the lapses of potential temperature and specific humidity are held constant.

The vertical distribution of the mean variables U, V, U_g, V_g, Θ_l, Q_w, and N must be specified initially. We discuss the specific choices made for each numerical experiment later. Initial values of the turbulence moments must also be selected in order to proceed with the numerical integration of Eqs. (6)–(9). Clearly we do not usually have enough information to specify accurate initial profiles of the turbulence variables. Therefore we go through a spin-up period in which the turbulence variables are permitted to adjust to the mean fields. This procedure is described further in Burk (1980).

c. Surface aerosol fluxes

It is generally believed that the bursting of bubbles at the sea surface is the primary mechanism responsible for the generation of salt aerosol. The major source of bubble production involves breaking waves and the associated whitecaps. Blanchard and Woodcock (1957) studied the bubble size distribution which develops when a wave entrains large amounts of air as it breaks. These bubbles, upon bursting, convert surface free energy into kinetic energy of jets of water which are unstable and break into drops which typically are roughly one-tenth of the original bubble diameter.

Monahan and his colleagues (Monahan, 1968, 1971; Monahan and Zietlow, 1969; Monahan *et al.*, 1982; Monahan *et al.*, 1983a and b) have developed a two-pronged attack in their investigation of the generation flux of salt aerosol at the sea surface. First, they have conducted photographic studies of the fractional sea surface coverage of whitecaps as a function of wind speed. Second, they use a laboratory whitecap simulation tank to measure the change in concentration of aerosol droplets per increment droplet radius associated with a wave breaking event. These wave tank results are also used to determine a time constant which characterizes the decay rate of a whitecap foam patch. Combining results from these studies, Monahan *et al.* (1983a) propose that the surface aerosol generation rate be given by

$$P_1 = 1.373U^{3.41}r^{-3}(1 + 0.057r^{1.05}) \times 10^{1.19\exp(-B^2)} \tag{18}$$

where r is the radius in microns at a standard relative humidity of 80 percent, U is the 10-meter wind speed in m s^{-1}, P is in units of m^{-2} s^{-1} μm^{-1}, and $B = (0.38 - \log r)/0.65$. Equation (18) is the form for upward aerosol flux at the surface that we use in this investigation. Figure 1 displays the behavior of the function P_1, rewritten as a volume flux. Note that as the wind speed changes, the shape of this production function does not change—the relative flux of large particles to small particles does not change with increasing winds. We will return to this important feature of (18) later in the paper.

Expressions for the deposition of particles to the sea surface also involve considerable complexity. In a turbulent flow carrying giant-sized particles (1–25 μm in our context) over a smooth surface, major contributors to the deposition flux are the fluctuating velocity component normal to the surface and gravitational sedimentation. Particles diffuse like a gas provided they can follow the accelerations of the turbulent eddies. In the main body of the ABL, diffusion is governed by the large eddies whose turnover time is roughly l/q. Particles in the range 1–30 μm adjust their velocity through Stokes drag to an imposed fluid velocity in a $1/e$ time of $\tau \sim w_s/g$,

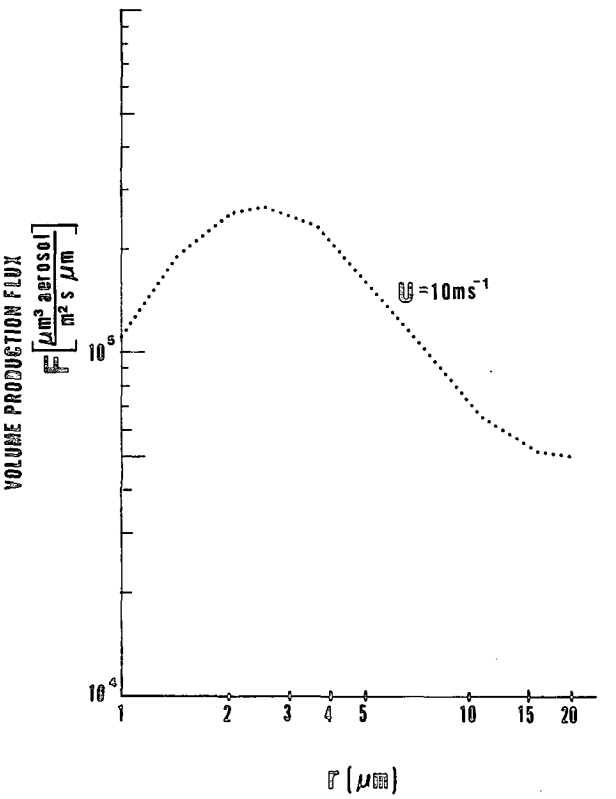

FIG. 1. Sea surface salt volume production flux proposed by Monahan *et al.* (1983a) and used in this study. Here the function is evaluated at a wind speed of 10 m s^{-1}.

where w_s is the Stokes fall speed (Friedlander, 1977, p. 96). Lewellen and Sheng (1980) show that for typical ABL values of l and q, $\tau \ll l/q$ for heights greater than a fraction of a meter. Thus, except very near the surface, particles in this size range will track the eddy motions and hence diffuse in the same manner as gas.

Although no complete theory of turbulent deposition exists, Friedlander (1977) develops an approximate expression in which particles in the bulk of the turbulent layer migrate by eddy diffusion to within one stop-distance, s, of the surface, where

$$s \sim u_0\tau = \frac{2}{9}\frac{\rho_p r^2 u_0}{\mu} \tag{19}$$

and u_0 is a characteristic velocity, taken as the fluctuating velocity just outside the viscous sublayer. The particles are then deposited by inertial impaction across the sublayer. Lewellen and Sheng develop a similar expression for deposition velocity,

$$v_d = K_2\frac{q^2\tau}{\delta}\left[1 - \exp\left(-K_3\frac{s}{\delta}\right)\right] + w_s. \tag{20}$$

The first term represents deposition due to inertial impaction in which $\frac{1}{2}q^2$ is the TKE just outside the

sublayer, and the exponential term represents a damping factor on these velocity fluctuations which depends upon the Stokes number (which is the ratio of stopping distance s to sublayer thickness δ). The second term represents deposition due to gravitational sedimentation. The empirical constants K_2 and K_3 are given in Lewellen and Sheng (1980). We use Eq. (20) as part of our lower boundary condition to Eq. (5).

d. Particle growth with humidity

In computing the condensational growth of the salt particles, we use the local mean relative humidity. This assumes that the particles adjust rapidly to quasi-equilibrium sizes as they fall into regions of differing ambient humidity. Toba (1965) investigates the validity of this equilibrium assumption. To do so, he examines the aerosol diffusional growth equation for different size salt particles and compares the growth rates for these particles falling through specified humidity gradients with their fall rates. Toba shows that, except in the case of large particles (>15 μm) in regions where the relative humidity is greater than 99%, rapid adjustment to changing ambient conditions is a good approximation.

The expression we use for equilibrium aerosol size is given by Kasten (1969) as

$$r(\mathrm{RH}) = r(0)(1 - \mathrm{RH})^{-0.26}, \qquad (21)$$

where RH is the relative humidity (fractional rather than percentage), and $r(0)$ is the salt particle dry radius.

In using the *mean* relative humidity in Eq. (21) we further assume that turbulent moisture fluctuations do not greatly alter the results. Since we carry the equation for moisture variance, $\overline{q_w^2}$, we are able to check this assumption. Our results show that turbulent moisture fluctuations generally result in relative humidity fluctuations of about one percent. Neglect of this contribution seems acceptable in view of other uncertainties in our problem.

3. Model experiments

a. Dry, neutral, steady-state ABLs

We begin with an uncomplicated set of numerical experiments which simulate the development of the sea-salt distribution towards a quasi-equilibrium. Starting with a dry, aerosol-free, neutral boundary layer with a fixed geostrophic wind speed, we integrate through one inertial period at which point the model's wind and turbulence fields develop Ekman-like profiles. (True Ekman profiles arise from assuming a constant eddy coefficient, which we have not done). During this period of the integration the surface aerosol flux P is set to zero. We do not want the development of the aerosol distribution to depend on the details of the surface stress and turbulence fields during the period when the model is dynamically developing its ABL. Simulations are run at three different geostrophic wind speeds, chosen so as to give Beaufort force (BF) 3, 5 and 7 winds at 10 m.

The normalized horizontal velocity components for the different geostrophic values are plotted in Fig. 2 as a function of scaled height. With a fixed roughness length we would expect the wind profiles to attain a so-called Rossby-similarity in which the Rossby number, $R_0 = U_g/(z_0 f)$, is the only parameter needed to characterize the wind distribution. This situation seems to be only approximately true here where z_0 varies with u_* as the boundary layer develops. The height in Fig. 2 is normalized by the quantity U_g/f, which is proportional to the neutral ABL depth, and then multiplied by 10^2 to give more convenient non-dimensional units for plotting. Table 1 contains important model output from these three equilibrium cases, with values taken from the end of the integration (one inertial period = 17.5 h). The values of the BF3 and BF5 Rossby numbers in Table 1 are very close to one another, but the normalized V components (Fig. 2b) are notably different, which is indicative of the past history of development and u_*-dependence of z_0 for the two cases.

Having attained the given Ekman-like profile (Fig. 2), we fix the mean wind profiles so as to avoid inertial oscillations. We then activate the surface production function (Eq. (18)), and sea-salt particles are generated, turbulently transported throughout the ABL, and deposited at the surface. (Thus, similar to a laboratory wind tunnel experiment that one might conduct, we fix the external forcing functions and permit the boundary layer to fully develop before turning on the aerosol generator.)

The integration continues until the aerosol distribution approaches steady state. For large particles this equilibrium is attained primarily by the concentration increasing until a balance between the upward production flux and the downward deposition flux is achieved. At the small size end of the distribution, near steady state is reached when the concentration increases to the point where the surface production flux can add little to the existing column abundance during the time frame of interest (hours).

Model-developed volume distributions for several Ekman-like layers of different wind speed (and hence different ABL depths) are shown in Fig. 3. Also shown in Fig. 3 are Woodcock's (1953) classic distributions measured at different Beaufort force winds. Plotted are the volume distributions adjusted to a standard 80% relative humidity versus the equilibrium radius at 80%. Such a humidity normalization procedure has become relatively common practice and is described in detail by Fairall *et al.* (1983). We choose to use volume distributions because they provide a more stringent method of observing simi-

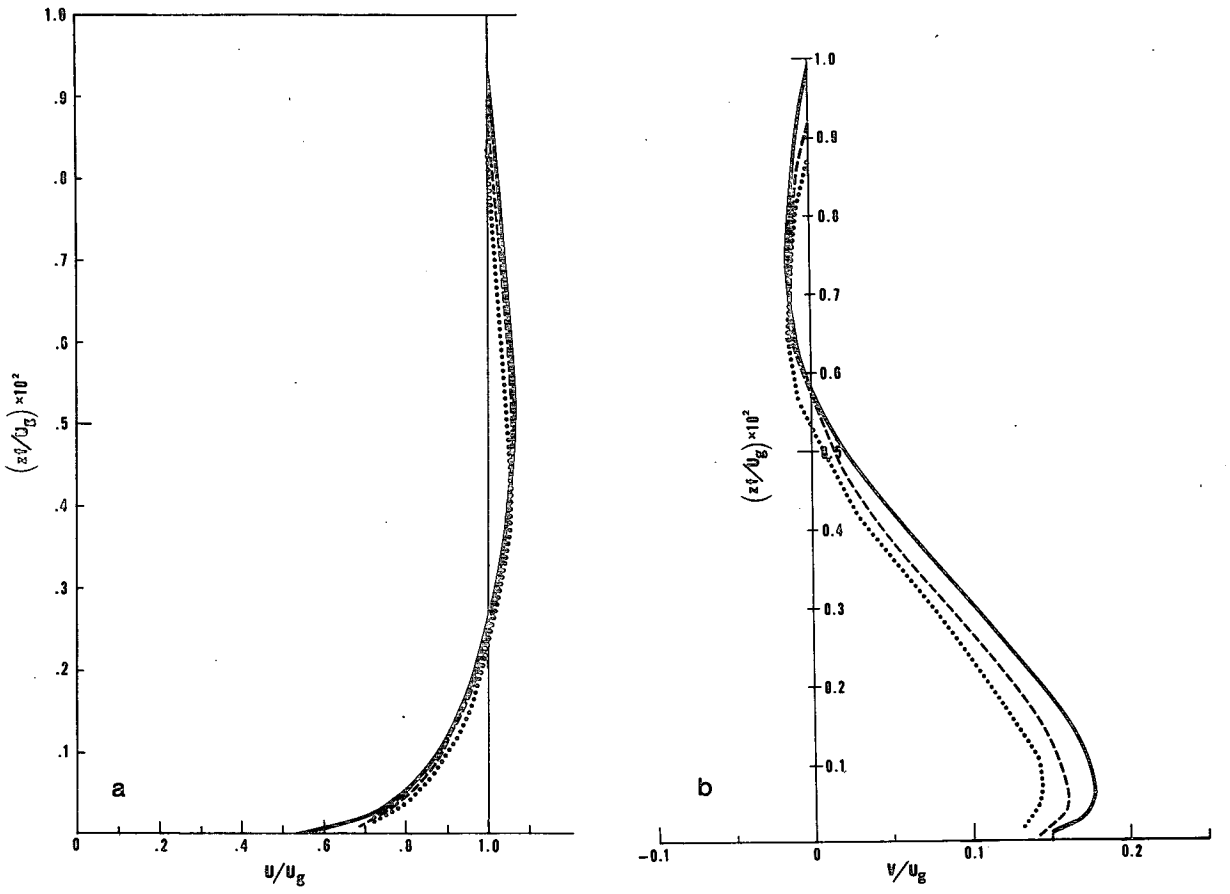

FIG. 2. Normalized wind components for steady state BF3 (dotted line), BF5 (dashed line), and BF7 (solid line) ABLs: (a) westerly component, (b) northerly component.

larities and differences in spectra than do $dN/d\log r$ versus r plots, which have very steep slopes.

The computed volume distributions shown in Fig. 3 are taken from a near surface (25 m) grid point, whereas the Woodcock data were collected at altitudes of 600–800 m in clear regions of the trade wind ABL windward of the Hawaiian Islands. In terms of *magnitude* and *shape*, the model distributions bear striking resemblance to the measurements, which is rather remarkable considering we have let these distributions develop from an initially aerosol-free state.

Sea-salt particle distributions at several heights in the BF5 ABL are shown in Fig. 4. There is less than a factor of 3 difference in volume concentration between 25 and 600 m at the small size end of the spectrum, while more than several orders of magnitude difference in volume concentration between these heights at the largest size considered. The trade wind regime where Woodcock took his measurements would typically be unstably stratified, with buoyant thermals providing convective mixing that is absent in the present simulations. Thus, the Woodcock distributions at 600–800 m should not differ greatly from near surface distributions.

The model distributions shown in Fig. 3, however, display no tendency for the peak to move towards larger radii with increasing wind force. Part of this discrepancy with Woodcock's observations may arise from the fact that, as noted in Section 2.c, our production function does not change shape with wind

TABLE 1. Model values important for Rossby scaling and diagnosis.

Wind force	10 m wind speed (m s^{-1})	U_g (m s^{-1})	u_* (m s^{-1})	z_0 (m)	R_0
BF3	4.5	6.0	0.15	2.55×10^{-4}	2.35×10^{8}
BF5	9.2	13.5	0.33	5.50×10^{-4}	2.45×10^{8}
BF7	15.5	25.5	0.64	2.1×10^{-3}	1.21×10^{8}

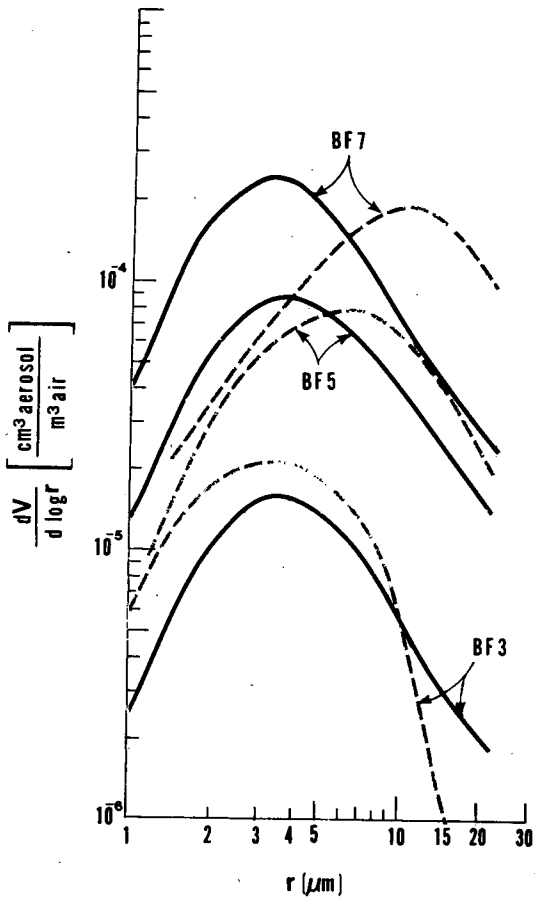

FIG. 3. Model computed volume distributions (solid lines) and measured results from Woodcock (1953) (dashed lines) at different Beaufort force (BF) winds.

speed, the peak staying at 2.5 μm, and also from our looking only at steady state distributions. We will see shortly that these distributions undergo substantial deformation when we consider nonsteady conditions. There is an added complication, however. Some more recent measurements of sea-salt spectra do not agree with Woodcock (1953). Patterson *et al.* (1980, Fig. 7) do not find any shift in the peak of the distribution with increasing wind force. At present the source of this discrepancy is unclear.

For particles larger than about 7 μm in dry radius, we find that the near surface number concentration is accurately given by $N = P/v_d$, which expresses the production-deposition equilibrium attained at the large end of the spectrum. Figure 5 shows the vertical distribution of 1 and 10 μm particles in the neutral, BF5 ABL. Clearly the 10 μm particles are not as well mixed as the 1 μm particles. Also shown is the height dependence, $(z/z_0)^{-w_f/ku_*}$, of the surface layer sedimentation-turbulent transport balance expression that is valid for the large particle end of the spectrum to about one-tenth of the ABL depth. This expression is derived from integration of the steady state version of Eq. (5); namely,

$$ku_* z \frac{\partial N}{\partial z} + W_f N = C, \tag{22}$$

where in the neutral surface layer $K = ku_* z$, C is a constant of integration, and we have set the vertical velocity W to zero. Clearly we cannot expect this expression to hold above the surface layer where the eddy coefficient no longer increases linearly with height, nor can we expect such a balance to exist for the small end of the spectrum where the fall speeds are negligible.

We choose to use neutral ABL simulations for observing the influence of wind speed on the aerosol spectra because it eliminates the complicating effect of buoyancy on the turbulent transport. Later we do conduct a trade wind simulation having a convective boundary layer, but present results only for a single simulation. Although we did run this case with various wind speeds, it was not clear how to meaningfully compare results from one simulation to another. The

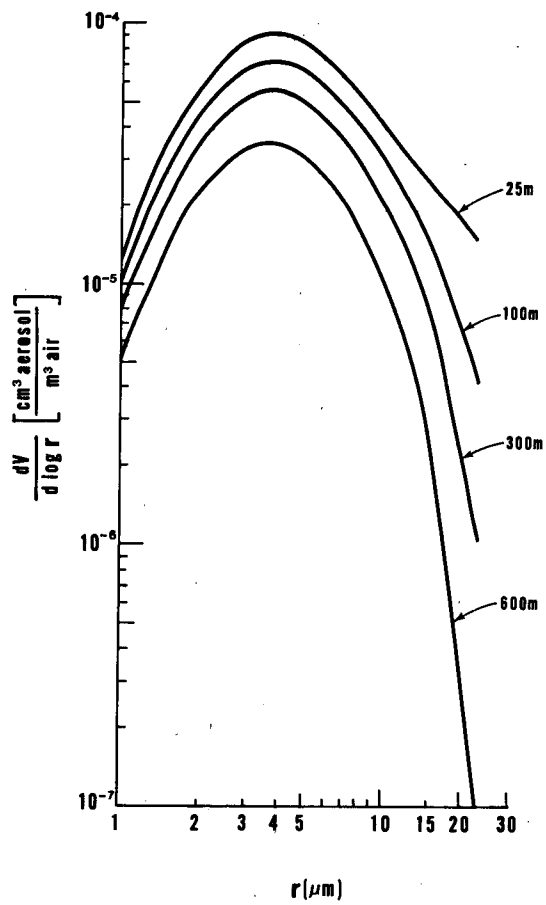

FIG. 4. Volume distributions at indicated heights in model-simulated BF5 ABL.

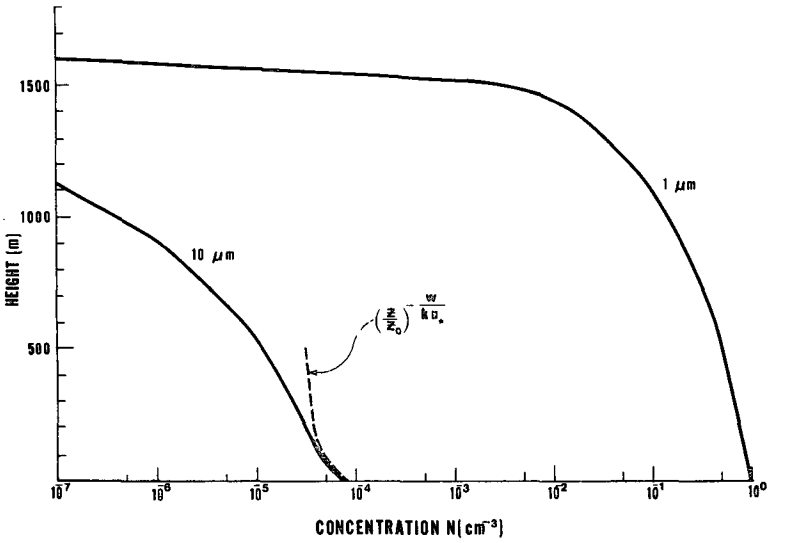

FIG. 5. Vertical distribution of 1 and 10 μm dry radii particles (1.5 and 15 μm at standard 80% relative humidity) in BF5 ABL. Dashed line shows height dependence of sedimentation-turbulence transport balance in the surface layer.

ratio of inversion height to Monin-Obukhov length, z_i/L, which indicates the degree of convective instability, varies from one simulation to the next. Even the profile of relative humidity, important to sedimentation, changes; thus simply labelling the spectra by wind speed and ignoring the impact of all other meteorological factors seems inadequate for the convective ABL, whether discussing model or observational results.

b. Simple synoptic wind speed variations

Having attained some understanding of the nature of the aerosol equilibrium distribution, we now turn to more meteorologically interesting cases in which the wind speed is changing with time. In order not to mask important features, we keep the wind speed variations simple. In the first of these simulations, the geostrophic wind is taken constant with height at a value which gives BF3 at 10 m, increases linearly to BF5 during a 3 h period, and then remains fixed. In the second simulation there is a ramp function *decrease* from BF5 to BF3.

The aerosol concentration is spun-up to its equilibrium value (at either BF3 or BF5) before the ramp change in wind speed begins. Once the geostrophic wind is altered, the changes in wind shear affect the eddy transport, and the aerosol production and deposition are altered [Eqs. (18) and (20)].

Figure 6 shows results for the case in which the BF increases from three to five, with curves labeled in hours after the beginning of the ramp function. Also shown for reference purposes is the BF5 equilibrium curve from Fig. 3. Because the actual wind

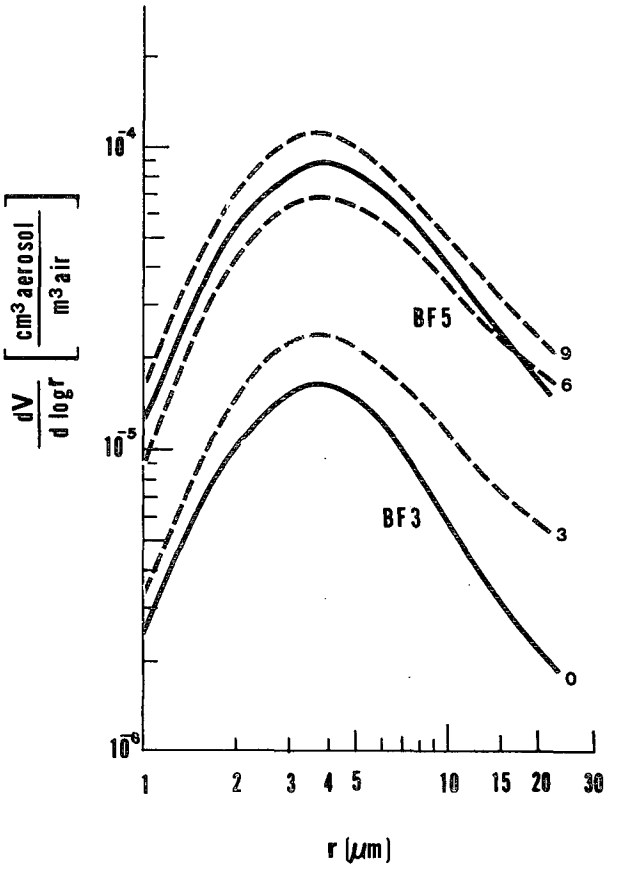

FIG. 6. Volume distribution response when wind undergoes ramp function increase from BF3 (4.4 m s^{-1} at 10 m) to BF5 (9.3 m s^{-1} at 10 m) during a 3 h period. Time labeled in hours after ramp function begins. Solid lines are steady state distributions.

undergoes an inertial oscillation that is initiated by the time varying geostrophic wind, the aerosol volume distribution actually exceeds its BF5 equilibrium value at hour 9; but, in general, the shape of the volume distribution is not distorted during this period of increasing winds.

We turn now to model results when the wind decreases (Fig. 7). Here there is a much greater deformation of the aerosol distribution. Because of their significant settling velocity, the concentration of large particles rapidly tracks the diminishing production function. During this period of decreasing winds the deposition flux excess causes the near surface concentration to drop, and an actual concentration inversion occurs in the vertical distribution of particles at the large end of our spectrum. Because of their long residence time, the concentration of small aerosols responds much more slowly to the diminishing surface generation flux. As a consequence, we expect substantial distortion of the size distribution following periods of diminishing winds.

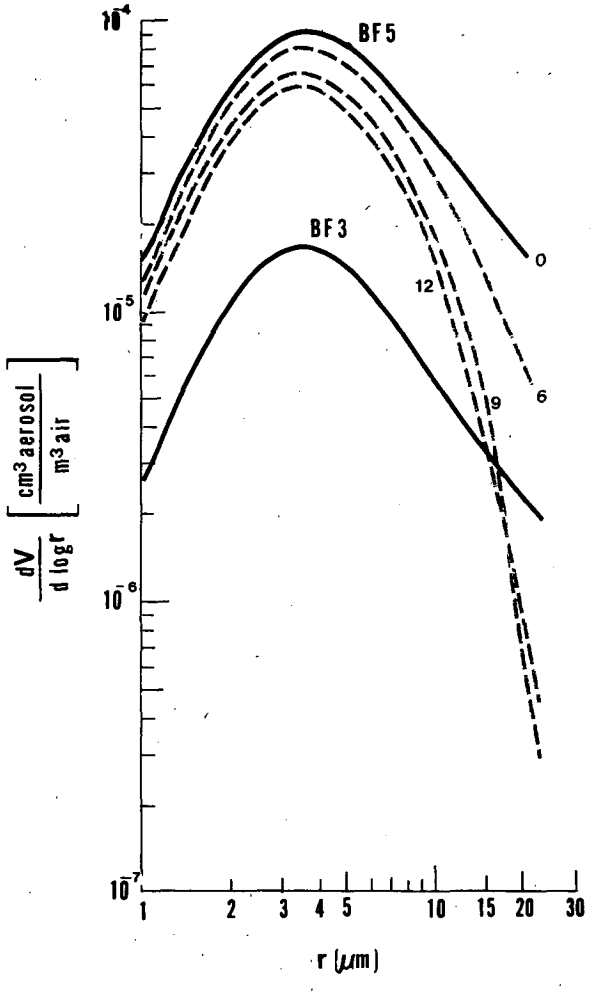

FIG. 7. As in Fig. 6 except ramp in wind *decreases* from BF5 to BF3 during 3 h period.

The model dynamics thus gives us a useful way to examine the rate at which different portions of the volume spectra adjust to changing meteorological conditions. Empirical methods which attempt to specify the distribution based solely on local conditions (e.g., Wells *et al.*, 1977) take no account of such nonsteady dynamics in the spectra. Using the average wind speed at a given location during the past 12 h say, should generally improve results based on such empirical models. It would be more desirable, however, to know wind trajectories and perhaps examine averages of the production function evaluated along the trajectory.

c. Humid, trade wind boundary layer simulation

Here we examine a case in which aerosol growth as a function of humidity is important. For initial conditions we use the trade wind vertical temperature, moisture, and wind profiles discussed by Sommeria (1976). In this simulation the surface layer is unstably stratified and convective transport is strong due to buoyancy forces. The relative humidity near the surface is 80%, increases to 85% in mid-boundary layer, reaches 95% just beneath the trade wind inversion, and then is very dry aloft. Integration proceeds until a quasi-equilibrium volume distribution is attained (about 12 h simulation time).

Figure 8 shows the aerosol volume distribution at several different heights in this trade wind ABL. Note that if the aerosols were well-mixed throughout the ABL, then these three curves would coincide. Instead, beyond 10 μm the vertical aerosol distribution deviates substantially from being well mixed. Further, recall that these curves have been adjusted to a standard of 80% relative humidity before plotting. If plotted in terms of actual wet volume at the local relative humidity versus local wet radius of the particle we find that the volume distribution actually shows an *increase* aloft in the high humidity region just beneath the trade wind inversion (Fig. 9). This has significant implications since, for example, it is the actual wet aerosol size that interacts with the radiation field to produce haze layers. Thus, although it is convenient to normalize spectra to a constant relative humidity, the fact that relative humidity is not a well-mixed property of the ABL has a profound impact on the manner in which aerosols interact with their environment.

4. Concluding remarks

In this study we couple a boundary layer turbulence model with empirical expressions for the generation and deposition of the sea-salt aerosol, thereby permitting examination of the development and dynam-

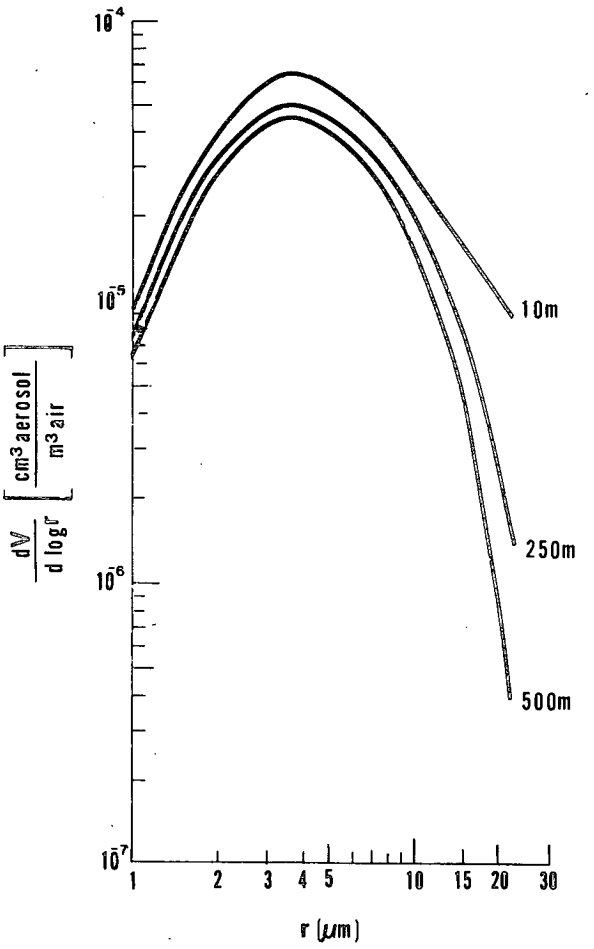

FIG. 8. Model computed volume distributions at different heights in a trade wind ABL simulation.

ics of marine aerosol volume distributions. We show that, starting from an aerosol-free state, equilibrium volume distributions which are realistic in magnitude and shape can be developed by the model at different values of Beaufort force winds. Unlike the Woodcock observations, however, our steady state distributions show no tendency for the peak to move towards larger radii with increasing wind speed. Patterson *et al.* (1980) do not find a spectral shift in their measurements (see their Fig. 7), but their spectra are much narrower than either Woodcock's or our model results.

As noted previously, the Monahan *et al.* (1983a) expression for the surface aerosol flux associated with whitecaps (Eq. 18) does not change shape with changing wind speed. There is evidence however that the peak in surface generation actually moves towards larger radii with increasing wind speed (Ross and Cardone, 1974; Wang and Street, 1978; Fairall *et al.*, 1983). Monahan *et al.* (1983b) point to the generation of spume drops by direct disruption of wave crests as becoming a significant additional aerosol production mechanism for wind speeds near 10 m s^{-1} and greater. In a preliminary attempt to quantify this additional generation flux they propose the expression

$$P_2 = \begin{cases} 0, & r < 10\ \mu\text{m} \\ 8.6 \times 10^{-6}\, e^{2.08U} r^{-2}, & 10 \leqslant r < 75\ \mu\text{m} \end{cases} \tag{23}$$

which is to be added to P_1 in Eq. (18) to yield the total production flux.

But such an arbitrary, abrupt transition in production as occurs in Eq. (23) at a radius of 10 μm is undesirable. Furthermore, when we used Eq. (23) and integrated to a steady state as in Section 3a, the concentration of particles larger than 10 μm at BF7 was many orders of magnitude too great. Thus, our results indicate that the exponential dependence on wind speed in Eq. (23) is far too drastic.

We ran the model with some simple synoptic variations in the wind speed to study the time-dependent reaction of the aerosol distribution. With increasing winds the volume distribution was little altered from its equilibrium shape, seeming to simply make a smooth transition from the equilibrium shape at the low wind speed to that at the higher speed. During our simulations of dying wind situations, however, the aerosol spectra became badly distorted

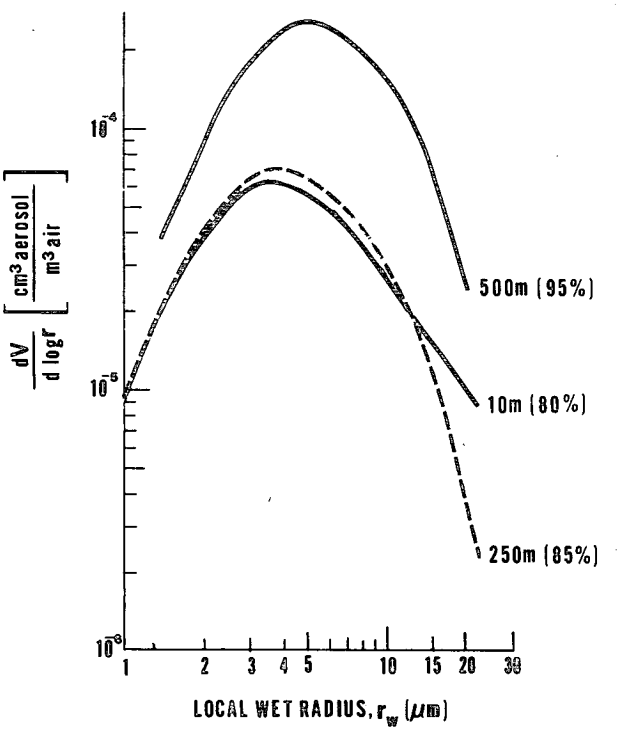

FIG. 9. As in Fig. 8 except plotted in terms of the wet radius at the local relative humidity rather than being normalized to a standard 80% humidity.

as compared to their equilibrium counterparts. Although these general features could perhaps have been anticipated, the model permits detailed examination of the dynamics of this aerosol distribution altering process.

Particles with dry radius greater than about 7 μm have sufficient settling speeds so that their concentration tracks variations in surface production quite rapidly. The residence time of particles smaller than this is too great to respond quickly to such variations. Empirical models which claim to be capable of defining the aerosol distribution as a function solely of local meteorological conditions must be regarded with considerable skepticism for this smaller size end of the spectrum. Regional models capable of forecasting the history of an air mass are required for determining local concentrations of the small-sized particles, although even here the method of proper initialization of aerosol content over the forecast domain is uncertain.

Finally, we examine the nature of computed equilibrium aerosol distributions in a humid, trade wind ABL. Blanchard (1983) and Blanchard and Woodcock (1980) present evidence for a "sea salt inversion layer" in the clear, trade wind air between clouds at an altitude of 600–800 m. That is, they find cases in which the cumulative salt content (μg m^{-3}) has a secondary maximum aloft just beneath the altitude of cloud base. The relative humidity in our simulation has a significant peak (95%) near 500 m, and our model-developed volume distribution, when based on local wet radius, shows a pronounced increase in this layer aloft. However, when normalized to a uniform 80% relative humidity at all altitudes, there is no sea salt-volume inversion in our simulation.

Acknowledgments. I am grateful to Dr. W. S. Lewellen for helpful comments on this manuscript.

APPENDIX

List of Symbols[2]

Roman symbols

$(A_1, A_2, B_1, B_2, C_1)$	closure constants from Mellor and Yamada (1982) (= 0.92, 0.74, 16.6, 10.1, 0.08)
C	constant of integration in Eq. (22)
f	Coriolis parameter
g	acceleration of gravity
k	von Karman's constant (taken = 0.35)
K	effective eddy coefficient for aerosol transport
K_1, K_2	coefficients from Lewellen and Sheng (1980) in deposition velocity expression, Eq. (20)
l	length scale of energy-carrying eddies
L	Monin-Obukhov length
N	aerosol concentration
p	fluctuating pressure
P_1	empirical sea-salt production flux expression developed by Monahan *et al.* (1983a)
P_2	surface production flux of large particles at high winds due to wave disruption
q^2	twice the turbulent kinetic energy
Q_w	total moisture (vapor plus liquid)
Q_r	radiative heating/cooling rates
RH	relative humidity
r	sea-salt aerosol radius
s	Stokes particle stopping distance (Friedlander, 1977, p. 96)
t	time
U, V	eastward and northward directed wind components, respectively
U_g, V_g	eastward and northward directed geostrophic wind components, respectively
V_d	deposition velocity
u_*	surface friction velocity
u_0	characteristic velocity outside viscous sublayer
W	vertical wind component
W_f	aerosol fall speed
x_i	Cartesian coordinates (x, y, z)
z	vertical coordinate

Greek symbols

α	angle of surface wind relative to x-axis
β	thermal expansion coefficient, $=1/\Theta_v$
γ	constant in down gradient diffusion closures, $=0.23$
δ	viscous sublayer thickness
Θ	potential temperature
μ	dynamic viscosity of air
ν	kinematic viscosity of air
ρ	aerosol droplet density
τ	e^{-1} speed decrease time for particle projected into stationary air
ϕ	nondimensional wind shear similarity function

Other symbols

$(\bar{\ })$	ensemble average
$(\ )_v$	virtual

[2] For mean values of variables we use upper case, while for turbulent fluctuations we use lower case.

REFERENCES

Blanchard, D. C., 1983: The production, distribution, and bacterial enrichment of the sea-salt aerosol. *Air-Sea Exchange of Gases and Particles,* Liss and Slinn, Eds., Reidel, 407–454.

——, and A. H. Woodcock, 1957: Bubble formation and modification in the sea and its meteorological significance. *Tellus,* **9,** 145–158.

——, and ——, 1980: The production, concentration and vertical distribution of the sea-salt aerosol. *Annals N.Y. Acad. Sci.*, **338,** 330–347.

Burk, S. D., 1977: The moist boundary layer with a higher order turbulence closure model. *J. Atmos. Sci.*, **34,** 629–638.

——, 1980: Refractive index structure parameters: Time-dependent calculations using a numerical boundary layer model. *J. Appl. Meteor.*, **19,** 562–576.

——, 1981: Comparison of structure parameter scaling expressions with turbulence closure model predictions. *J. Atmos. Sci.*, **38,** 751–761.

——, and W. T. Thompson, 1982: Operational evaluation of a turbulence closure model forecast system. *Mon. Wea. Rev.*, **110,** 1535–1543.

Businger, J. A., 1973: Turbulent transfer in the atmospheric surface layer. *Workshop on Micrometeorology,* D. Haugen, Ed., Amer. Meteor. Soc., 67–100.

Donaldson, C. duP., 1973: Construction of a dynamic model of the production of atmospheric turbulence and the dispersal of atmospheric pollutants. *Workshop on Micrometeorology,* D. Haugen, Ed., Amer. Meteor. Soc., 313–392.

Fairall, C. W., K. L. Davidson and G. E. Schacher, 1983: An analysis of the surface production of sea-salt aerosols. *Tellus,* **35B,** 31–39.

Friedlander, S. K., 1960: Similarity considerations for the particle-size spectrum of a coagulating, sedimenting aerosol. *J. Meteor.*, **17,** 479–483.

——, 1977: *Smoke, Dust and Haze.* Wiley and Sons, 317 pp.

Junge, C. E., 1957: The vertical distribution of aerosols over the ocean. *Artificial Stimulation of Rain,* Pergamon, 89–96.

Kasten, F., 1969: Visibility forecast in the phase of precondensation. *Tellus,* **21,** 631–635.

Lewellen, W. S., and Y. P. Sheng, 1980: Modeling of dry deposition of SO_2 and sulfate aerosols. EPRI EA-1452, Project 1306-1, 67 pp.

Mack, E. J., C. W. Rogers and B. J. Wattle, 1983: An evaluation of marine fog forecast concepts. Calspan Rept. No. 6866-M-1, Calspan Corp., Buffalo, NY, 73 pp.

Mellor, G. L., 1973: Analytic prediction of the properties of stratified planetary surface layers. *J. Atmos. Sci.*, **30,** 1061–1069.

——, and T. Yamada, 1974: A hierarchy of turbulence closure models for planetary boundary layers. *J. Atmos. Sci.*, **31,** 1791–1806.

——, and ——, 1982: Development of a turbulence closure model for geophysical fluid problems. *Rev. Geophys. Space Phys.*, **20,** 851–875.

Monahan, E. C., 1968: Sea spray as a function of low elevation wind speed. *J. Geophys. Res.*, **73,** 1127–1137.

——, 1971: Oceanic whitecaps. *J. Phys. Oceanogr.*, **1,** 139–144.

——, and C. R. Zietlow, 1969: Laboratory comparisons of fresh-water and salt-water whitecaps. *J. Geophys. Res.*, **74,** 6961–6966.

——, K. L. Davidson and D. E. Spiel, 1982: Whitecap aerosol productivity deduced from simulation tank measurements. *J. Geophys. Res.*, **87,** 8898–8904.

——, D. E. Spiel and K. L. Davidson, 1983a: Model of marine aerosol generation via whitecaps and wave disruption. *Ninth Conf. Aerospace and Aeronautical Meteorology,* Amer. Meteor. Soc., 147–152.

——, C. W. Fairall, K. L. Davidson and P. J. Boyle, 1983b: Observed inter-relations between 10 m winds, ocean whitecaps and marine aerosols. *Quart. J. Roy. Meteor. Soc.*, **109,** 379–392.

Patterson, E. M., C. S. Kiang, A. C. Delany, A. F. Wartburg, A. C. D. Leslie and B. J. Huebert, 1980: Global measurements of aerosols in remote continental and marine regions: Concentrations, size distributions, and optical properties. *J. Geophys. Res.*, **85,** 7361–7376.

Ross, D. B., and V. Cardone, 1974: Observations of oceanic whitecaps and their relation to remote measurements of surface wind speed. *J. Geophys. Res.*, **79,** 444–452.

Sato, K., 1979: Effect of diffusion-sedimentation and washout processes on aerosol size distributions. *J. Meteor. Soc. Jap.*, **57,** 432–442.

Sommeria, G., 1976: Three-dimensional simulation of turbulent processes in an undisturbed trade wind boundary layer. *J. Atmos. Sci.*, **33,** 216–241.

Toba, Y., 1965: On the giant sea-salt particles in the atmosphere: II. Theory of the vertical distribution in the 10-m layer over the ocean. *Tellus,* **17,** 365–382.

Wang, C. S., and R. L. Street, 1978: Transfers across an air-water interface at high wind speeds: The effect of spray. *J. Geophys. Res.*, **83,** 2959–2969.

Wells, W. C., G. Gal and M. W. Munn, 1977: Aerosol distributions in maritime air and predicted scattering coefficients in the infrared. *Appl. Opt.*, **16,** 654–659.

Woodcock, A. H., 1950: Sea salt in a tropical storm. *J. Meteor.*, **7,** 397–401.

——, 1953: Salt nuclei in marine air as a function of altitude and wind force. *J. Meteor.*, **10,** 362–371.

——, and M. M. Gifford, 1949: Sampling atmospheric sea-salt nuclei over the ocean. *J. Mar. Res.*, **8,** 177–197.

Yamada, T., 1978: A three-dimensional, second-order closure numerical model of mesoscale circulations in the lower atmosphere. ANL/RER-78-1, Argonne Natl. Lab., 67 pp.